Check for updates

Space Weather

RESEARCH ARTICLE
10.1029/2025SW004538

Regional Medium-Scale Traveling Ionospheric Disturbance Propagation Model Based on BDS GEO Satellites

Dengkui Mei[1], Xiaohong Zhang[1,2,3], Xiaodong Ren[2,3], Xuan Le[2], Wentao Yang[2], and Ahmed Abdelaziz[4,5]

[1]Chinese Antarctic Center of Surveying and Mapping, Wuhan University, Wuhan, China, [2]School of Geodesy and Geomatics, Wuhan University, Wuhan, China, [3]Hubei Luojia Laboratory, Wuhan University, Wuhan, China, [4]State Key Laboratory of Information Engineering in Surveying, Mapping and Remote Sensing Wuhan University, Wuhan, China, [5]Faculty of Engineering, Benha University, Benha, Egypt

Key Points:

- A Singular Spectrum Analysis algorithm was developed to reconstruct missing BeiDou GEO TEC data
- A regional MSTID propagation model was established for the first time based on BDS GEO TEC data
- The propagation model reduced TID-induced ionospheric delay errors by 40.7%–55%

Correspondence to:
X. Zhang,
xhzhang@whu.edu.cn

Citation:
Mei, D., Zhang, X., Ren, X., Le, X., Yang, W., & Abdelaziz, A. (2026). Regional medium-scale traveling ionospheric disturbance propagation model based on BDS GEO satellites. *Space Weather*, *24*, e2025SW004538. https://doi.org/10.1029/2025SW004538

Received 14 MAY 2025
Accepted 8 DEC 2025

Author Contributions:
Conceptualization: Dengkui Mei, Xiaohong Zhang
Data curation: Xuan Le, Wentao Yang, Ahmed Abdelaziz
Formal analysis: Xuan Le
Funding acquisition: Xiaohong Zhang, Xiaodong Ren
Methodology: Dengkui Mei
Software: Dengkui Mei
Supervision: Xiaohong Zhang, Xiaodong Ren
Visualization: Wentao Yang, Ahmed Abdelaziz
Writing – original draft: Dengkui Mei
Writing – review & editing: Xiaodong Ren

Abstract Accurate modeling of traveling ionospheric disturbances (TIDs) is essential for characterizing their spatiotemporal variations and mitigating their effects on Global Navigation Satellite System (GNSS) precise positioning. This study develops a regional medium-scale TID (MSTID) propagation model using BeiDou geostationary orbit (GEO) total electron content (TEC) data. First, we propose a singular spectrum analysis (SSA)-based interpolation method to reconstruct the possible data gaps of BDS GEO TEC time series, enhancing its TID detection stability. Second, we select well-distributed GNSS reference stations in Hong Kong, grouping them into triplets to estimate average TID parameters (main frequency, amplitude, velocity, and direction) using cross-spectral analysis. Finally, a regional MSTID propagation model is constructed using a cosine function, incorporating the average phases, frequency, and amplitudes. The model was firstly validated through the measured TID signal from the HKSC, HKST, and HKKT stations on 29 October 2018. Results indicate strong agreement between the model-estimated and measured TID signals. Validation results show the model reduces TID-induced ionospheric delay errors by 48.2%, 50.3%, and 42.7% without accounting for the time lag and further by 55.0%, 53.1%, and 45.1% with optimal temporal alignment for HKSC, HKST, and HKKT, respectively. Another MSTID event on 30 April 2016, was also selected to further validate the general applicability of the proposed TID model under different propagation characteristics. It confirms the model's accuracy and reliability. This study provides an effective approach for precise TID characterization and supports mitigation strategies for GNSS positioning errors caused by traveling ionospheric disturbances.

Plain Language Summary Traveling ionospheric disturbances (TIDs) are wave-like variations in the ionosphere that can distort satellite signals and degrade the accuracy of Global Navigation Satellite Systems (GNSS), such as GPS and BeiDou. These disturbances introduce rapid fluctuations in the ionospheric electron density, leading to positioning errors in high-precision GNSS applications like real-time navigation and precision agriculture. Given the increasing reliance on GNSS for critical infrastructure and emerging technologies, improving TID modeling is essential to enhance positioning resilience under disturbed ionospheric conditions. BeiDou Geostationary Orbit (GEO) satellites offer unique advantages for TID monitoring because they provide stable and continuous observations of ionospheric disturbances. Leveraging these observations, this study develops a regional medium-scale TID propagation model to characterize and mitigate disturbance effects on GNSS positioning. This research advances both scientific understanding of ionospheric dynamics and practical solutions for more reliable satellite navigation.

1. Introduction

Traveling ionospheric disturbances (TID) are propagating plasma density fluctuations in the ionosphere, exhibiting a broad spectrum of velocities and frequencies (Hernández-Pajares et al., 2006; Tsugawa et al., 2007). Large-scale TIDs (LSTIDs) are predominantly driven by magnetospheric energy input during geomagnetic storms, and their occurrence rate exhibits a clear positive correlation with solar activity (Ding et al., 2007; Hajkowicz, 1990). In contrast, medium-scale TIDs (MSTIDs) show no such dependence and they can occur during both high and low solar activity periods (Kotake et al., 2006, 2007). The excitation of MSTIDs has been attributed to several mechanisms. Specifically, a primary source is the upward propagation of neutral atmospheric gravity waves (AGWs) from the lower atmosphere, which can seed perturbations that evolve into daytime MSTIDs (Frissell et al., 2016; Tsuboi et al., 2023). At mid- and low latitudes, plasma instabilities—notably the

© 2026. The Author(s).
This is an open access article under the terms of the Creative Commons Attribution-NonCommercial-NoDerivs License, which permits use and distribution in any medium, provided the original work is properly cited, the use is non-commercial and no modifications or adaptations are made.

15427390, 2026, 1, Downloaded from https://agupubs.onlinelibrary.wiley.com/doi/10.1029/2025SW004538 by Trinity Health Ann Arbor, Wiley Online Library on [01/04/2026]. See the Terms and Conditions (https://onlinelibrary.wiley.com/terms-and-conditions) on Wiley Online Library for rules of use; OA articles are governed by the applicable Creative Commons License

Perkins instability (Perkins, 1973)—provide another generation mechanism, effectively triggering some nighttime MSTIDs under favorable conditions (Kelley, 2011; Shiokawa et al., 2003). Furthermore, the electric field perturbations originating from the sporadic E (Es) layer can map along geomagnetic field lines to the F-region, thereby initiating MSTIDs (Liu et al., 2019).

These TID disturbances induce significant perturbations in background ionospheric electron density, posing severe challenges to high-precision Global Navigation Satellite System (GNSS) positioning (Belehaki et al., 2020; Jia et al., 2024; Paziewski et al., 2022; Yang & Morton, 2020), particularly in years of high solar activity. Multi-scale and rapidly evolving TIDs pose significant impacts on high-precision GNSS positioning techniques, particularly affecting real-time kinematics (RTK) (Hernández-Pajares et al., 2017; Timoté et al., 2020) and precise point positioning real-time kinematic (PPP-RTK) positioning performance (Li et al., 2022; Zhang et al., 2022). The impact is especially pronounced for the PPP-RTK positioning technique, which critically depends on accurate ionospheric delay corrections.

Traditional ground-based ionospheric monitoring instruments (e.g., ionosondes, radars) face limitations in spatiotemporal coverage due to their restricted detection ranges and sparse distribution, hindering comprehensive TID detections. In contrast, the dense GNSS networks have emerged as a powerful tool for TID detection by capturing quasi-periodic signatures in total electron content (TEC) measurements (Huang et al., 2018; Tang, 2023; Yang et al., 2017). However, most TID-related studies primarily focus on qualitative analysis of spatiotemporal propagation characteristics and disturbance mechanisms (Belehaki et al., 2020; Chen et al., 2020; Mei et al., 2025; Ren et al., 2022; Zakharenkova et al., 2016; Zhai et al., 2025), few efforts have been devoted to developing quantitative TID propagation models. Establishing such models is critical for mitigating TID-induced positioning errors, yet the lack of robust mathematical representations remains a key challenge. The wave-like propagation characteristics of TID, however, offer a theoretical foundation for model development.

Accurate estimation of TID propagation information (frequency, phase, amplitude) is essential for model construction. Although GPS (Global Positioning System) TEC data are widely used for TID detection, the Doppler effect—introduced by the rapid relative motion between GPS satellites and TIDs—makes it difficult for accurate parameter extraction. The BeiDou Navigation Satellite System (BDS) geostationary (GEO) satellites can overcome this limitation, as their fixed ionospheric pierce points (IPPs) minimize Doppler-induced errors (Huang et al., 2018). While techniques like the Galileo transform method can mitigate GPS Doppler effects (Wan et al., 1997), BDS GEO observations remain superior for TID studies. Consequently, researchers often employ the maximum entropy method (MEM), a robust cross-spectral analysis technique, for TID parameter estimation based on BDS GEO data (Huang et al., 2016, 2018, 2020). The implementation details of MEM have been comprehensively described in previous studies (Ding et al., 2011; Huang et al., 2016).

However, the possible interruptions of GNSS signals due to environmental factors or data transmission issues can lead to gaps in BDS GEO TEC time series in a whole day, hindering continuous TID monitoring. It was reported that the singular spectrum analysis (SSA), a nonparametric spectral method, has been proven effective for gap-filling in geophysical time series (Yi & Sneeuw, 2021a). In addition, the estimation of TID propagation parameters exhibits station-dependent variability (Huang et al., 2016). To avoid the influence of different station selection strategies on the estimation results of TID propagation parameters, those adjacent regional reference stations with good geometrical distribution are suggested to be selected and grouped into triplets for estimating parameters of TID events.

In this study, we first develop an SSA-based interpolation method to reconstruct complete BDS GEO TEC time series. Second, we optimize TID parameter estimation using BDS GEO observations based on the geometrically well-distributed stations. Finally, a regional ionospheric TID propagation model was constructed using cosine functions based on the phase, main frequency, and amplitude information of the regional TID event. The model is validated using both simulated and real TEC data, demonstrating its potential to mitigate ionospheric disturbances on precise positioning.

The paper is structured as follows: Section 1 introduces GNSS-based TID detections and modeling requirements. Section 2 details the TEC gap-filling method and TID model development. Section 3 evaluates

propagation model performances using both simulated and real TEC data, and Section 4 summarizes key findings and implications.

2. Data and Methods

This section presents the methodology, beginning with an overview of the Hong Kong GNSS Reference Station Network data. We then detail the BDS GEO TEC data interpolation algorithm for addressing missing observations and the establishment of the TID propagation model.

2.1. Data Description

The study utilizes GNSS observations from the Hong Kong GNSS Reference Station Network (SatRef), consisting of 19 Continuously Operating Reference Stations (CORS) with an average inter-station distance of 10–15 km. These stations are equipped with multi-GNSS receivers capable of tracking signals from BeiDou (BDS-2/BDS-3), GPS, Galileo, and GLONASS constellations. The network's capability to track BDS GEO satellites, combined with its 30-s sampling rate, provides exceptional resolution for traveling ionospheric disturbance monitoring in the region.

2.2. Filling GEO TEC Data Gap Using Singular Spectrum Analysis

BDS GEO TEC series occasionally contain data gaps due to receiver anomalies or environmental disturbances, including space weather effects (Banville & Langley, 2013; Basu et al., 2002; Lee et al., 2017; Li et al., 2021; Vilà-Valls et al., 2020). These missing observations require reconstruction to maintain the temporal continuity and integrity of BDS GEO TEC data for reliable TID monitoring.

Singular spectrum analysis offers an effective solution for data gap filling in TEC time series. This technique decomposes signals into interpretable components (trends, oscillations, and noise) based on variance contributions, enabling data reconstruction through temporal correlation analysis (Kondrashov & Ghil, 2006; Schoellhamer, 2001). Compared to machine learning methods that demand extensive training and computational resources (Li et al., 2020; Sun et al., 2019), SSA provides a computationally efficient alternative (Li et al., 2019). Its ability to reconstruct missing epochs based on the temporal structure of the available data makes it particularly suitable for restoring the continuity of BDS GEO TEC series. Moreover, its proven effectiveness in geophysical applications (Yi & Sneeuw, 2021a) further supports its applicability to GNSS-derived TEC data processing.

We implement an SSA-based gap-filling approach using the open-source framework developed by Yi and Sneeuw (2021b), ensuring reliable reconstruction of the BDS GEO TEC series for subsequent TID analysis.

2.3. TID Propagation Model

Following data gap filling, we processed the BDS GEO TEC series using a Savitzky-Golay (SG) filter to extract the continuous 24-hr detrended TEC (dTEC) series within a day. This least squares smoothing approach effectively preserves signal features while removing low-frequency trends (Chen et al., 2023; Gou et al., 2023). The dTEC series exhibits fluctuations during TID occurrence and is often used for TID detection.

For spectral analysis of TID signals in the dTEC series, wavelet transform provides excellent time-frequency localization, enabling precise identification of TID onset and duration; fast Fourier transform (FFT) offers robust spectral decomposition into sinusoidal components, delivering essential amplitude and phase information; and maximum entropy method (MEM) combines spectral resolution with phase preservation capabilities. While wavelet analysis excels in temporal localization of TID events, its inability to directly extract phase information necessitates complementary methods. We therefore employ FFT and MEM for accurate amplitude and phase estimation, which is critical for subsequent TID parameter estimation and TID modeling.

Figure 2 illustrates the phase differences observed in TID signals across different stations. The phase differences, derived from BDS GEO dTEC series, serve as the foundation for calculating TID propagation parameters through cross-spectral analysis (Ding et al., 2011; Huang et al., 2016). For optimal propagation parameter estimation of TID events, the three selected stations should not be distributed on the same straight line, that is, the three stations

15427390, 2026, 1, Downloaded from https://agupubs.onlinelibrary.wiley.com/doi/10.1029/2025SW004538 by Trinity Health Ann Arbor, Wiley Online Library on [01/04/2026]. See the Terms and Conditions (https://onlinelibrary.wiley.com/terms-and-conditions) on Wiley Online Library for rules of use; OA articles are governed by the applicable Creative Commons License

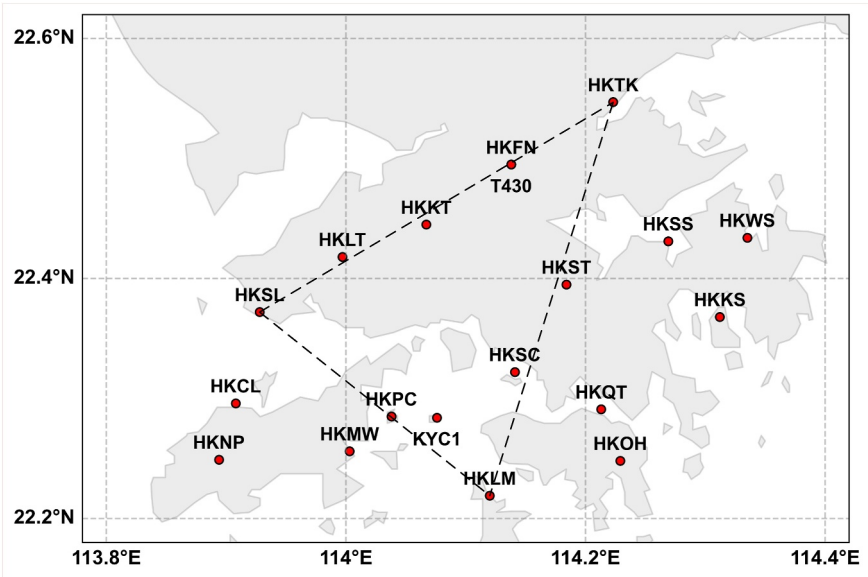

Figure 1. Distribution of CORS GNSS stations in Hong Kong.

should form a triangle (see dashed triangle in Figure 1), such as the southernmost (HKLM), western (HKSL), and northernmost (HKTK) stations. Figure 3 also illustrates the schematic representation of TID propagation, where stations 1, 2, 3, and 4 refer to stations HKLM, HKSL, HKTK, and HKSC, respectively. The phase differences between three stations are calculated for estimating the propagation parameters by using the cross-spectral method. The calculation procedure involves measuring phase differences between station pairs and applying cross-spectral analysis.

Due to the rapid propagation of traveling ionospheric disturbances, there are phase differences in the TID signals over three different GNSS stations, which satisfies the following relationships:

$$\begin{aligned} k_x x_{21} + k_y y_{21} &= \varphi_{21} \\ k_x x_{31} + k_y y_{31} &= \varphi_{31} \end{aligned} \tag{1}$$

where k_x and k_y are unknown horizontal wavenumbers in the x and y directions; (x_{21}, y_{21}) and (x_{31}, y_{31}) are the relative position relationships of three GNSS stations, that is, the plane coordinate difference; φ_{21} and φ_{31} are the phase differences of TID signals observed by adjacent stations.

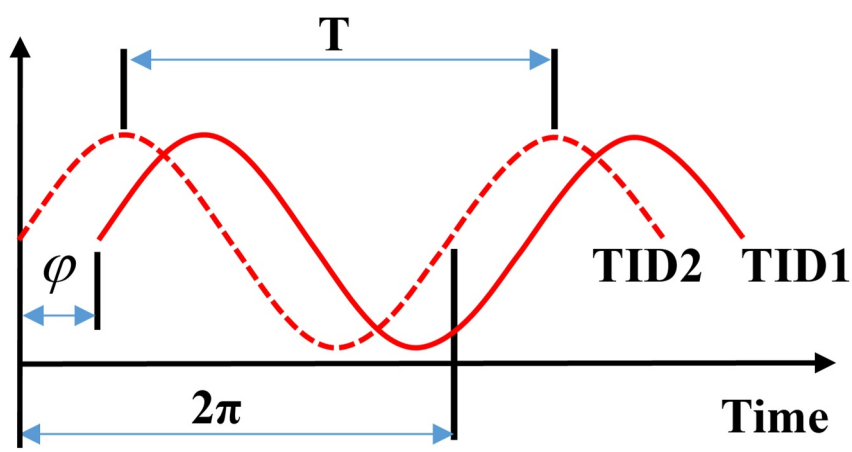

Figure 2. Schematic diagram of two TID signals with different initial phases.

15427390, 2026, 1, Downloaded from https://agupubs.onlinelibrary.wiley.com/doi/10.1029/2025SW004538 by Trinity Health Ann Arbor, Wiley Online Library on [01/04/2026]. See the Terms and Conditions (https://onlinelibrary.wiley.com/terms-and-conditions) on Wiley Online Library for rules of use; OA articles are governed by the applicable Creative Commons License

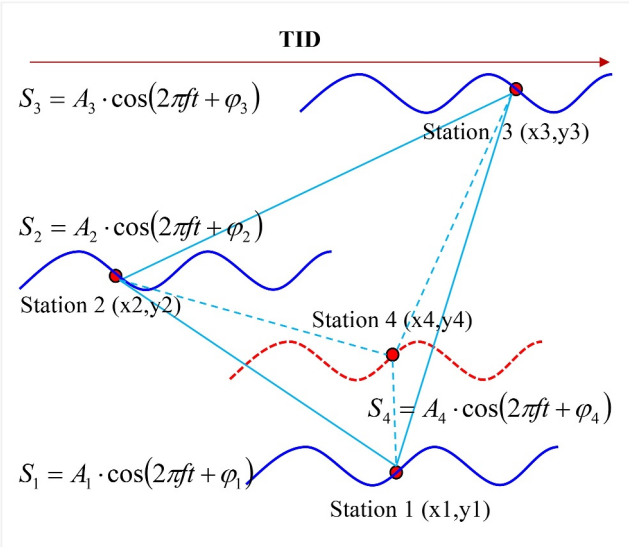

Figure 3. Schematic diagram of TID propagation model over different stations.

After obtaining k_x and k_y from the solution of Equation 1, the propagation parameters of TID such as horizontal phase velocity v, period T, horizontal wavelength λ and propagation azimuth σ are further calculated as follows:

$$\begin{aligned} v &= 2\pi f / \sqrt{{k_x}^2 + {k_y}^2} \\ T &= 1/f \\ \lambda &= vT \\ \sigma &= \arctan(k_x/k_y) \end{aligned} \tag{2}$$

where f is the main frequency of the TID signal.

The model construction involves three key steps: (a) Extraction of TID signals from BDS GEO detrended TEC time series across three reference stations; (b) According to the method described above, every three reference stations in the region are grouped into triplets to compute the TID propagation parameters in the region. (c) Integration of these parameters to establish the comprehensive propagation model.

Theoretically, rover station 4 is affected by the same TID event, then rover station 4 and reference station 1 also satisfy the following relationship:

$$\begin{aligned} k_x x_{41} + k_y y_{41} &= \varphi_{41} \\ \varphi_{41} &= \varphi_4 - \varphi_1 \end{aligned} \tag{3}$$

where φ_4 denotes the phase of the TID perturbation signal at rover station 4; x_{41} and y_{41} denote the coordinate differences between rover station 4 and reference station 1.

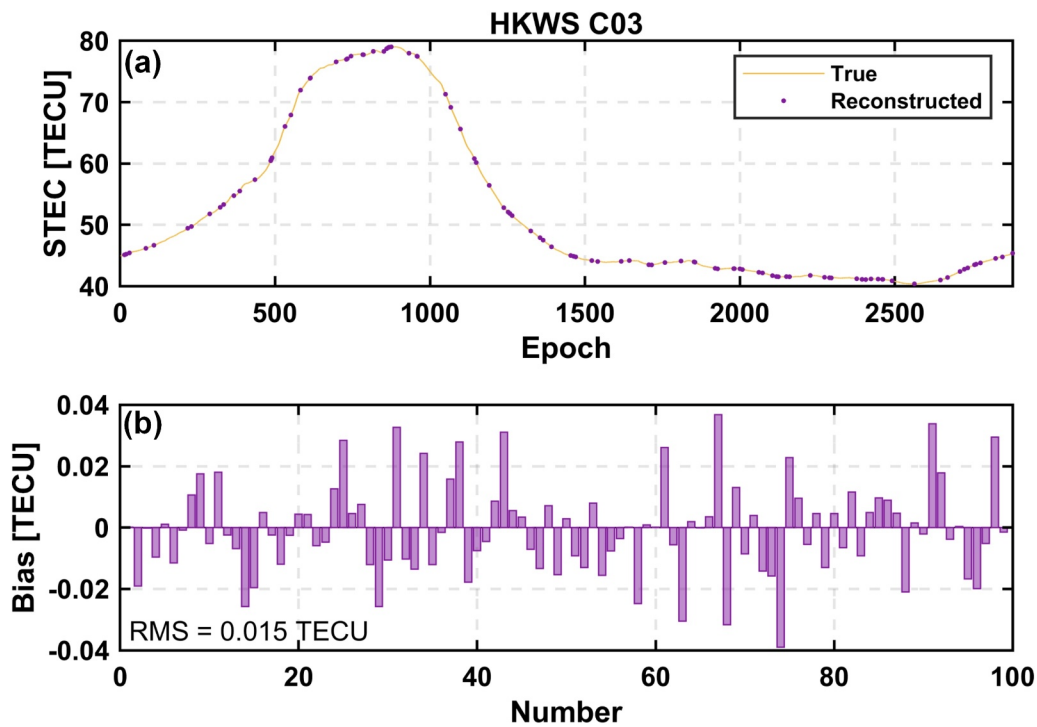

Figure 4. BDS GEO TEC data gap filling when artificially removing 100 epochs.

15427390, 2026, 1, Downloaded from https://agupubs.onlinelibrary.wiley.com/doi/10.1029/2025SW004538 by Trinity Health Ann Arbor, Wiley Online Library on [01/04/2026]. See the Terms and Conditions (https://onlinelibrary.wiley.com/terms-and-conditions) on Wiley Online Library for rules of use; OA articles are governed by the applicable Creative Commons License

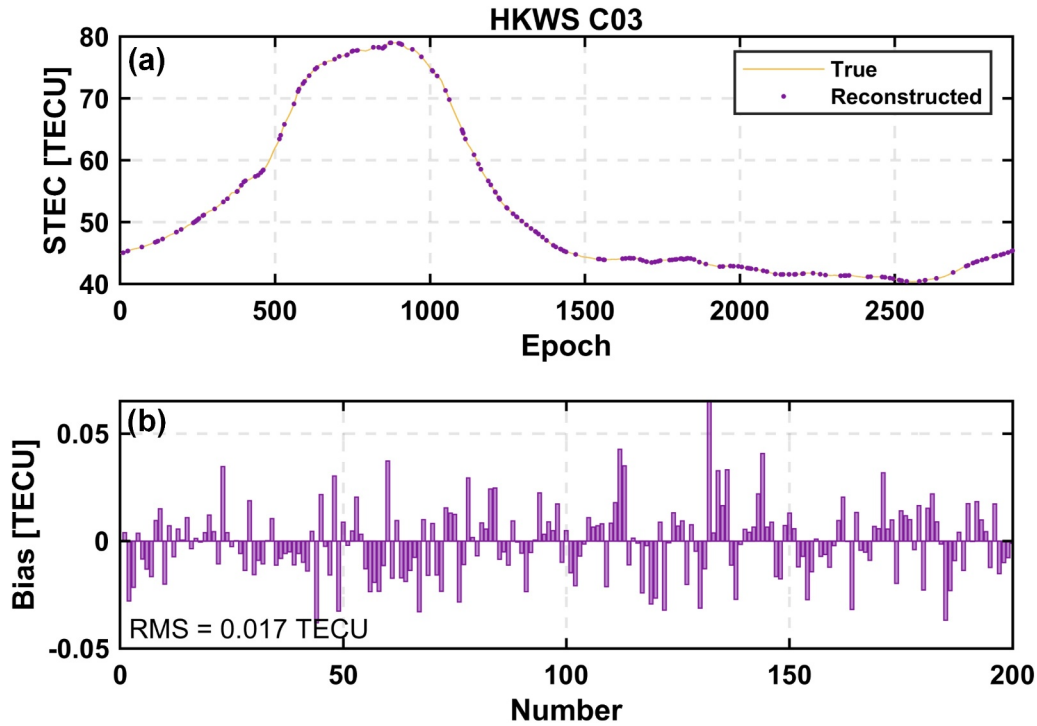

Figure 5. BDS GEO TEC data gap filling when artificially removing 200 epochs.

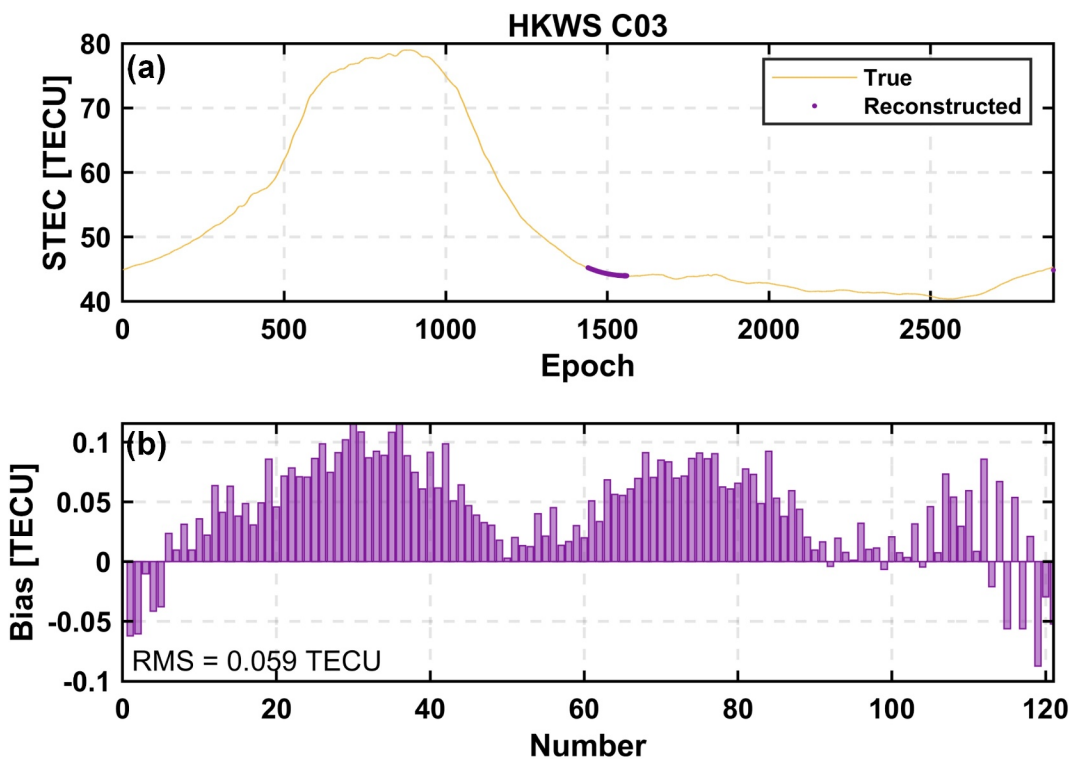

Figure 6. Reconstruction of 1-hr (120 epochs) continuous TEC gap between 12:00 UT and 13:00 UT.

15427390, 2026, 1, Downloaded from https://agupubs.onlinelibrary.wiley.com/doi/10.1029/2025SW004538 by Trinity Health Ann Arbor, Wiley Online Library on [01/04/2026]. See the Terms and Conditions (https://onlinelibrary.wiley.com/terms-and-conditions) on Wiley Online Library for rules of use; OA articles are governed by the applicable Creative Commons License

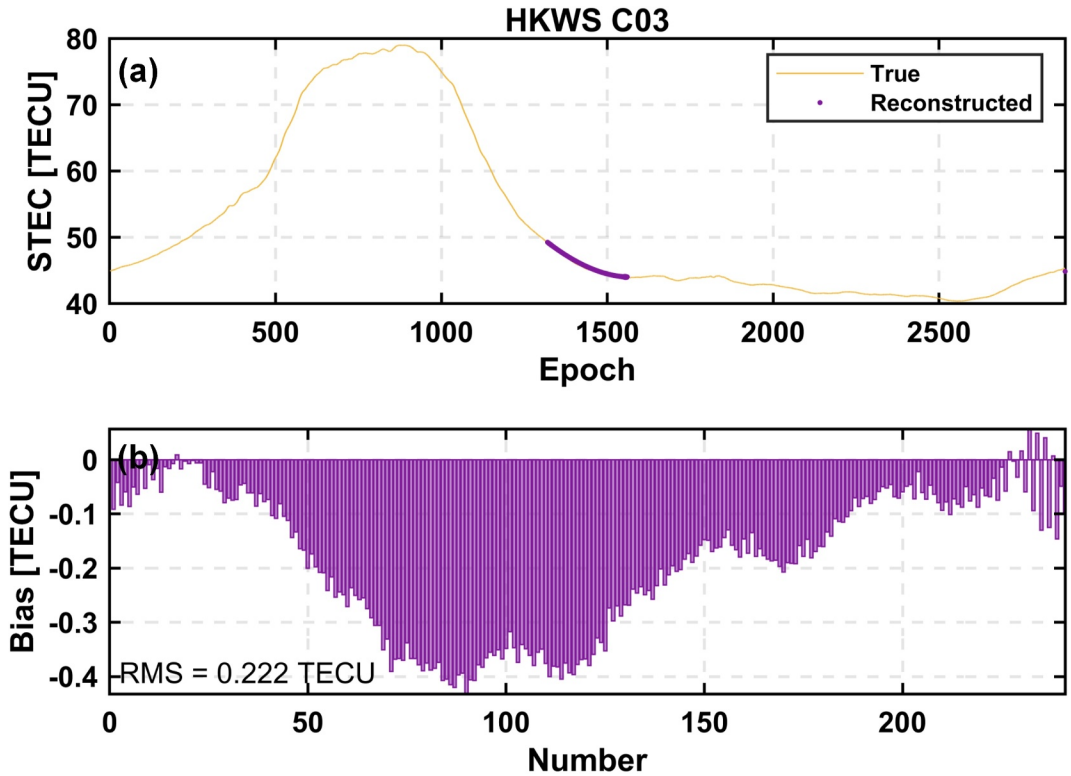

Figure 7. Reconstruction of 2-hr (240 epochs) continuous TEC gap between 11:00 UT and 13:00 UT.

According to the principle of the cross-spectral method for calculating TID propagation parameters, the horizontal wave numbers k_x and k_y in the x and y directions are calculated from Equation 1 as:

$$\begin{aligned} k_x &= \frac{y_{31}\varphi_{21} - y_{21}\varphi_{31}}{x_{21}y_{31} - x_{31}y_{21}} \\ k_y &= \frac{x_{31}\varphi_{21} - x_{21}\varphi_{31}}{x_{31}y_{21} - x_{21}y_{31}} \end{aligned} \tag{4}$$

Equation 4 is expressed in matrix form as:

$$\begin{bmatrix} k_x \\ k_y \end{bmatrix} = \begin{bmatrix} x_{21} & y_{21} \\ x_{31} & y_{31} \end{bmatrix}^{-1} \begin{bmatrix} \varphi_{21} \\ \varphi_{31} \end{bmatrix} \tag{5}$$

Substituting Equation 4 into Equation 3 yields the initial phase of the rover station 4 as:

$$\begin{aligned} \varphi_4 &= \varphi_1 + k_x x_{41} + k_y y_{41} \\ &= \varphi_1 + \frac{y_{31}\varphi_{21} - y_{21}\varphi_{31}}{x_{21}y_{31} - x_{31}y_{21}}(x_4 - x_1) + \frac{x_{31}\varphi_{21} - x_{21}\varphi_{31}}{x_{31}y_{21} - x_{21}y_{31}}(y_4 - y_1) \end{aligned} \tag{6}$$

When the initial phase of the TID signal at the rover station 4 is obtained, and the corresponding TID event propagation parameters such as the main frequency and amplitude, the TID propagation model is constructed according to Equation 7:

$$S_4 = A_4 \cos\left(2\pi f t + \varphi_4\right) \tag{7}$$

15427390, 2026, 1, Downloaded from https://agupubs.onlinelibrary.wiley.com/doi/10.1029/2025SW004538 by Trinity Health Ann Arbor, Wiley Online Library on [01/04/2026]. See the Terms and Conditions (https://onlinelibrary.wiley.com/terms-and-conditions) on Wiley Online Library for rules of use; OA articles are governed by the applicable Creative Commons License

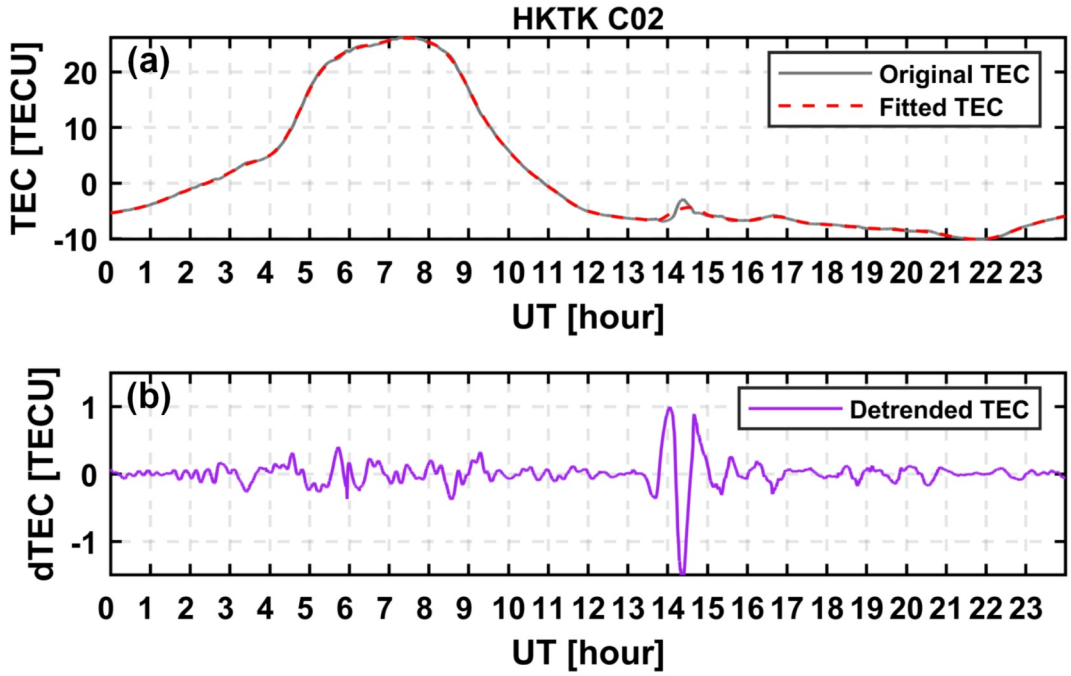

Figure 8. The TEC and dTEC time series observed by the C02 satellite at the HKTK station on 29 October 2018.

where f is the main frequency of the TID event; t is the time; φ_4 is the initial phase of the TID signal at the rover station 4; and A_4 denotes the amplitude of the TID perturbation at the rover station, which can generally be determined based on the average TID amplitudes at the other $(n-1)$ reference stations in the region:

$$A_n = \frac{A_1 + A_2 + \cdots + A_{n-1}}{n-1} \tag{8}$$

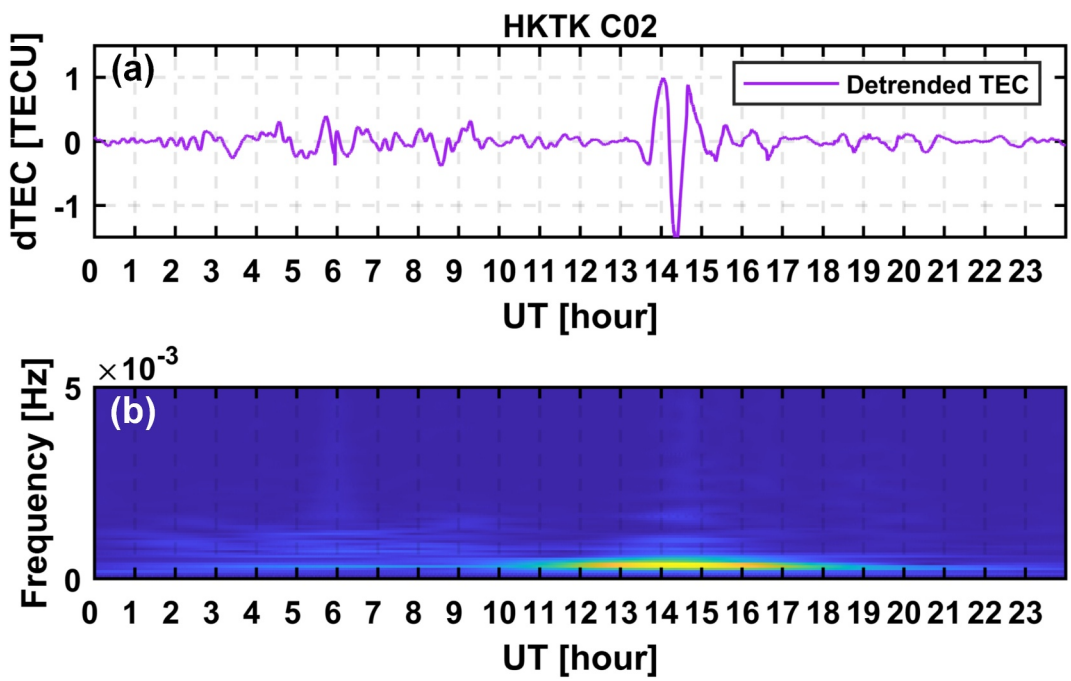

Figure 9. Spectral analysis of dTEC time series using wavelet transform at the HKTK station on 29 October 2018.

15427390, 2026, 1, Downloaded from https://agupubs.onlinelibrary.wiley.com/doi/10.1029/2025SW004538 by Trinity Health Ann Arbor, Wiley Online Library on [01/04/2026]. See the Terms and Conditions (https://onlinelibrary.wiley.com/terms-and-conditions) on Wiley Online Library for rules of use; OA articles are governed by the applicable Creative Commons License

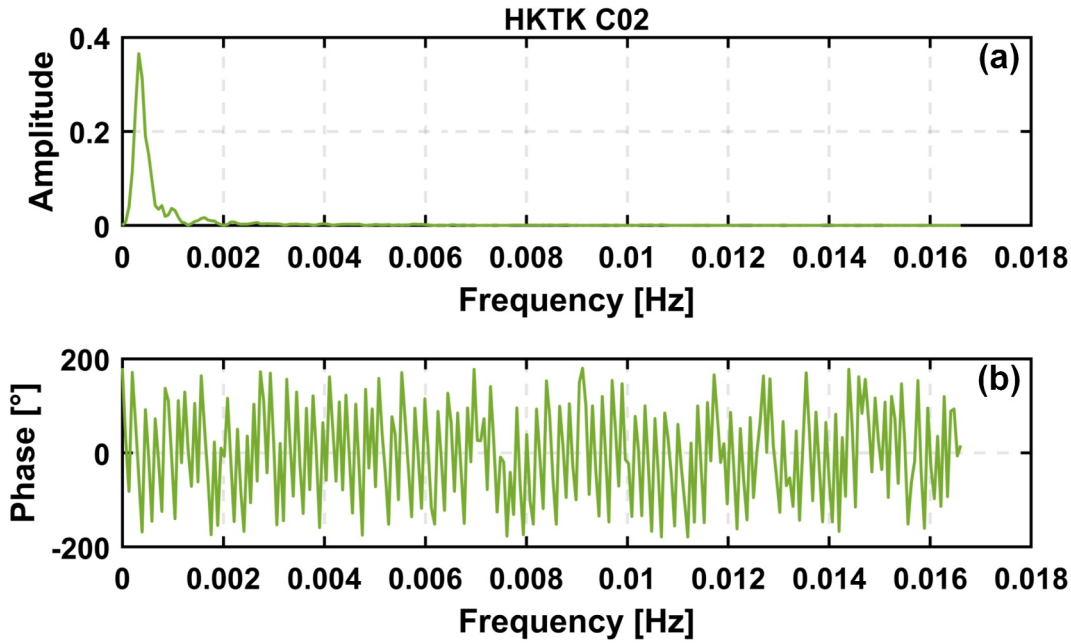

Figure 10. The amplitude and phase information of the dTEC sequence at the HKTK station on 29 October 2018.

3. Experiment Results and Discussion

This section systematically evaluates our proposed approach through two key components: (a) quantitative assessment of the SSA algorithm's interpolation performance for BDS GEO TEC time series reconstruction and (b) development of a TID propagation model and comprehensive validation using both simulated and real BDS GEO TEC observations.

3.1. Gap Filling of BDS GEO TEC Series

As mentioned above, to enable continuous monitoring of ionospheric TID events using BDS GEO TEC time series, we address possible data gaps through singular spectrum analysis. This approach effectively reconstructs missing TEC values while preserving the temporal characteristics of the original signal.

To validate the SSA algorithm's reliability, we conducted experiments by artificially removing 100 and 200 epochs from the original complete BDS GEO TEC series. Then we utilize the SSA algorithm to reconstruct the missing TEC values and compare them with the original true TEC values. Figures 4 and 5 show the BDS GEO TEC data gap filling when artificially removing 100 and 200 epochs, respectively. In Figures 4 and 5, the top panels refer to the original and reconstructed BDS TEC data, while bottom panels refer to the bias between the reconstruction results and the true values. The reconstruction results demonstrate the method's effectiveness, with RMS values of only 0.015 TECU and 0.017 TECU for the respective gap lengths when compared with the original true TEC values.

In addition to the two tests with randomly removed 100- and 200-epoch TEC segments, we conducted two additional experiments to evaluate the SSA method's performance under 1-hr (120 epochs) and 2-hr (240 epochs) continuous data gaps. As shown in Figures 6 and 7, validation results demonstrate robust performance of the SSA method across different gap durations, with the 1-hr continuous gap test showing very good reconstruction accuracy (RMS value is 0.059 TECU), while the 2-hr continuous gap test maintains reasonable accuracy (RMS value is 0.222 TECU).

These results demonstrate that the SSA method achieves consistent accuracy across both random and continuous gap scenarios. While the error increases with gap duration, it remains below 0.25 TECU even for 2-hr continuous outages, indicating a robust capability to reconstruct partially missing epochs in BDS GEO TEC data and thereby enhance the stability of TID detection. It should be noted, however, that this effectiveness is most pronounced

15427390, 2026, 1, Downloaded from https://agupubs.onlinelibrary.wiley.com/doi/10.1029/2025SW004538 by Trinity Health Ann Arbor, Wiley Online Library on [01/04/2026]. See the Terms and Conditions (https://onlinelibrary.wiley.com/terms-and-conditions) on Wiley Online Library for rules of use; OA articles are governed by the applicable Creative Commons License

15427390, 2026, 1, Downloaded from https://agupubs.onlinelibrary.wiley.com/doi/10.1029/2025SW004538 by Trinity Health Ann Arbor, Wiley Online Library on [01/04/2026]. See the Terms and Conditions (https://onlinelibrary.wiley.com/terms-and-conditions) on Wiley Online Library for rules of use; OA articles are governed by the applicable Creative Commons License

Table 1
TID Propagation Parameters Based on FFT Spectral Information for Different Station Combinations

Scheme	Frequency (Hz)	Period (min)	Velocity (m/s)	Wavelength (km)	Azimuth (°)
HKLM-HKSL-HKTK	0.000326	51.2	33.942	104.271	246.427
HKLT-HKNP-HKOH	0.000326	51.2	33.055	101.545	264.669
HKKS-HKKT-HKMW	0.000326	51.2	31.646	97.215	243.033
HKPC-HKTK-HKWS	0.000326	51.2	30.283	93.029	250.670
HKOH-HKST-HKWS	0.000326	51.2	37.093	113.957	258.770
Average	0.000326	51.2	33.204	102.003	252.714

under relatively stable ionospheric conditions. The method's tendency to produce overly smoothed results constitutes a key limitation, as it is likely inadequate for accurately reconstructing sharp fluctuations and fine-scale structures associated with intense ionospheric irregularities (e.g., plasma bubbles). In such scenarios, SSA provides a smoothed estimate rather than recovering the true physical variations. Consequently, the application of this method to periods or regions characterized by significant ionospheric irregularities should be approached with caution.

3.2. Estimation and Validation of TID Parameters

During a geomagnetically quiet period on 29 October 2018 (DOY302), Wu et al. (2021) reported two nighttime medium-scale TID events in low-latitude China using the all-sky airglow imager. One event exhibited northeast-to-southwest propagation, traversing the Hong Kong region. We analyzed this event using Hong Kong's CORS network data, extracting BDS GEO TEC time series and deriving dTEC series through SG filtering.

Figure 8 presents the original and detrended TEC series observed by the C02 satellite from station HKTK. In Figure 8, it can be seen that during the time of the TID occurrence, the dTEC series exhibits significant fluctuations, with the maximum amplitude exceeding 1 TECU, and the fluctuation contains at least one complete wave peak and trough. This TEC fluctuation, attributed to the nighttime TID, persisted until approximately 16:00 UT before gradually attenuating to background levels.

The dTEC series were analyzed using three spectrum analysis methods: fast Fourier transform (FFT), maximum entropy method, and wavelet transform. While FFT and MEM provide conventional spectral information, the wavelet transform offers distinct advantages by simultaneously resolving both time and frequency domains (see Figure 9). As shown in Figure 9, this dual-resolution capability enables precise identification of TID onset (13:00 UT) and duration (∼3 hr), as evidenced by the clear temporal correspondence between the wavelet spectrum and dTEC fluctuations at the HKTK station. The wavelet analysis reveals concentrated signal energy between 13:00 UT and 16:00 UT, consistent with the observed perturbation period in the dTEC series.

The wavelet transform can provide time-frequency information of the TID signal, but it lacks direct phase extraction capability. For accurate phase determination, the FFT method is more suitable as it decomposes signals into sinusoidal components, providing complete spectral information including both amplitude and phase

Table 2
TID Propagation Parameters Based on MEM Spectral Information for Different Station Combinations

Scheme	Frequency (Hz)	Period (min)	Velocity (m/s)	Wavelength (km)	Azimuth (°)
HKLM-HKSL-HKTK	0.000326	51.2	33.854	104.000	249.688
HKLT-HKNP-HKOH	0.000326	51.2	33.420	102.666	258.472
HKKS-HKKT-HKMW	0.000326	51.2	26.565	81.607	230.700
HKPC-HKTK-HKWS	0.000326	51.2	30.150	92.621	253.347
HKOH-HKST-HKWS	0.000326	51.2	35.001	107.523	265.204
Average	0.000326	51.2	31.798	97.683	251.482

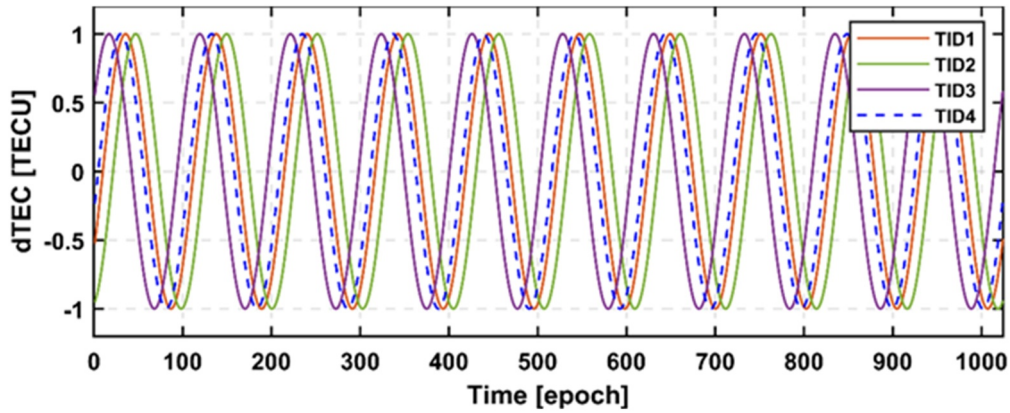

Figure 11. Estimation of rover station TID signals based on three reference stations' TID signals.

characteristics. This makes FFT particularly valuable for modeling TID propagation where precise phase relationships between stations are required.

Figure 10 displays the amplitude and phase spectra obtained through FFT analysis of the dTEC time series at the HKTK station. The analysis identified a primary TID frequency of 0.000326 Hz (corresponding to a period of 51.2 min) with a phase angle of −51.1°. Consistent spectral examination of HKSL and HKLM stations revealed matching dominant frequencies (phase angles of −158.1° and −121.8°, respectively), confirming these perturbations originated from the same TID event. Through cross-spectral analysis, we determined the TID propagation parameters to be as follows: a velocity of 38.730 m/s, a wavelength of 118.979 km, and a propagation direction of 248.022°.

To minimize potential biases in TID propagation parameter estimation caused by station geometry, only station combinations with good geometric distribution and comparable inter-station distances were considered for analysis. For instance, the HKNP-HKMW-HKLM combination was excluded due to suboptimal geometry. For each qualifying station combination, we independently calculated propagation parameters using cross-spectral

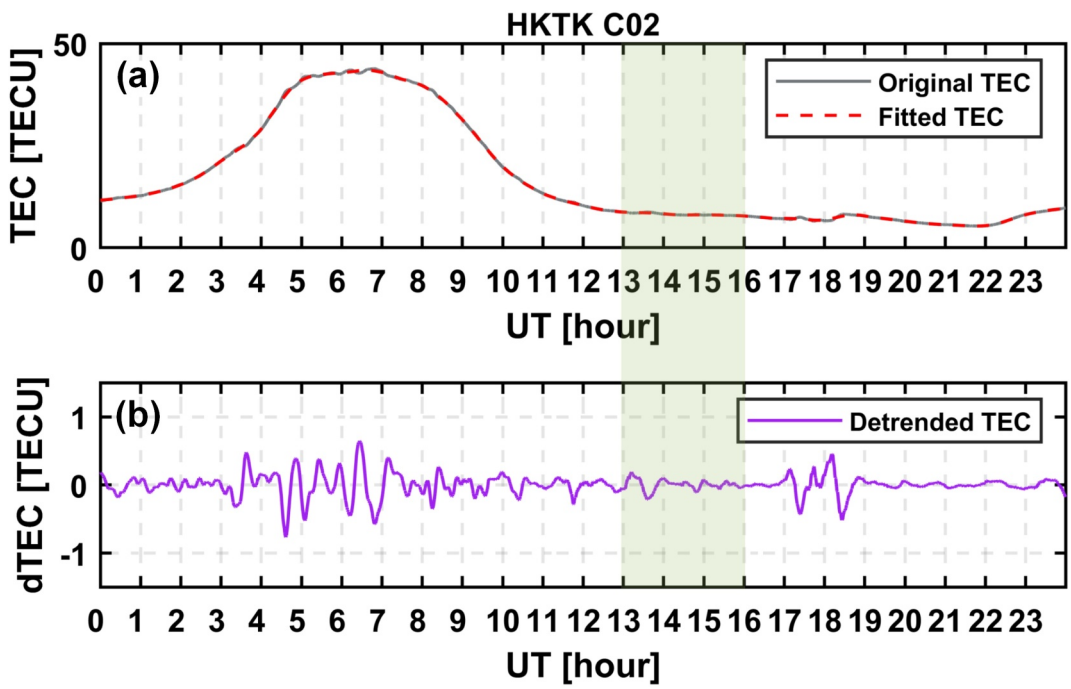

Figure 12. Detrended TEC time series estimated by HKTK station without TID occurrence on 28 October 2018.

15427390, 2026, 1, Downloaded from https://agupubs.onlinelibrary.wiley.com/doi/10.1029/2025SW004538 by Trinity Health Ann Arbor, Wiley Online Library on [01/04/2026]. See the Terms and Conditions (https://onlinelibrary.wiley.com/terms-and-conditions) on Wiley Online Library for rules of use; OA articles are governed by the applicable Creative Commons License

15427390, 2026, 1, Downloaded from https://agupubs.onlinelibrary.wiley.com/doi/10.1029/2025SW004538 by Trinity Health Ann Arbor, Wiley Online Library on [01/04/2026]. See the Terms and Conditions (https://onlinelibrary.wiley.com/terms-and-conditions) on Wiley Online Library for rules of use; OA articles are governed by the applicable Creative Commons License

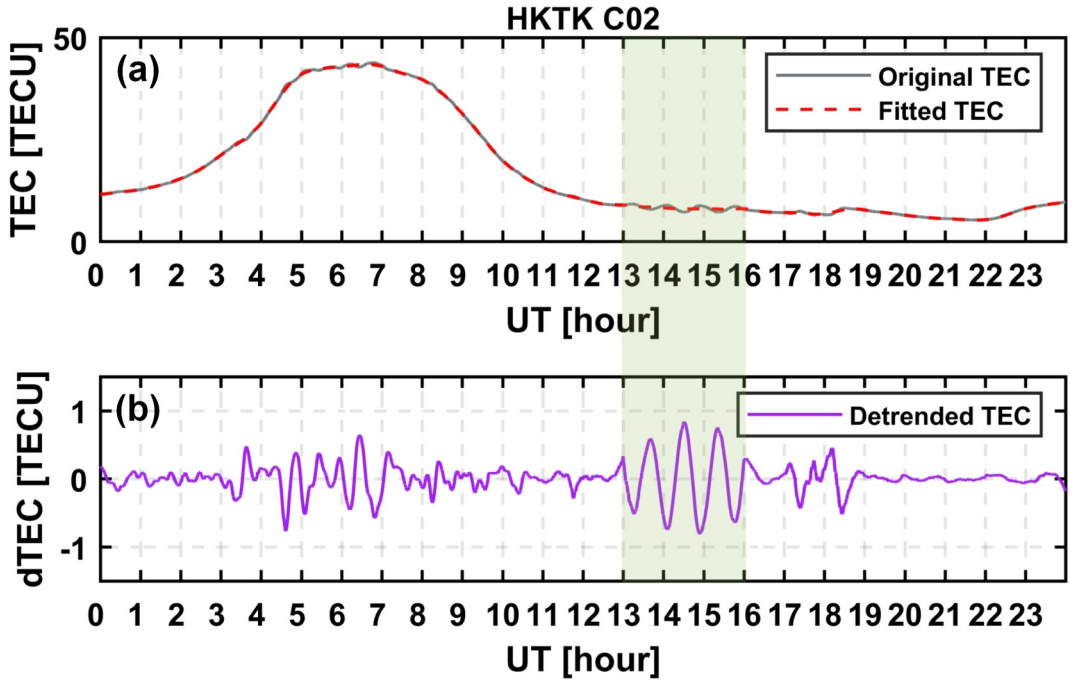

Figure 13. Detrended TEC time series at the HKTK station after adding model-estimated TID from 13:00 UT to 16:00 UT on 29 October 2018.

analysis. The final parameters were determined through averaging of those valid combinations, reducing spatial sampling errors, and improving estimation reliability.

For the nighttime TID event observed over China on 29 October 2018 (DOY 302), we applied both FFT and MEM methods to obtain amplitudes and phase differences across station combinations. Then the TID propagation parameters were estimated using cross-spectral analysis based on spectral information obtained by the FFT and MEM methods. The TID propagation parameters estimated based on FFT and MEM spectral information for different station combinations are given in Tables 1 and 2, respectively. The average propagation parameters calculated using FFT based on these station combinations are as follows: velocity is 33.204 m/s, wavelength is 102.003 km, and direction is 252.714°; the average propagation parameters calculated using MEM based on these station combinations are as follows: velocity is 31.798 m/s, wavelength is 97.683 km, and direction is 251.482°. The close agreement between these independent methods validates the robustness of our propagation parameter estimation approach. The estimated TID propagation speed values in this study are lower than typical MSTID propagation speeds from tens of meters per second to hundreds of meters per second, which may represent the special propagation characteristics of the observed TID. The detection results reported by Wu et al. (2021) indicated that the opposite interaction of MSTIDs with ionospheric irregularity structures may modified the propagation characteristics of MSTID structures.

Besides, as reported by Wu et al. (2021), the MSTID structures captured by the airglow imager consisted of multiple wavefronts. Airglow imaging provides superior horizontal resolution for detecting fine-scale wavefronts that may be blended in TEC measurements. GNSS-based detection results primarily captured the integrated TEC perturbations along satellite-receiver ray paths, which naturally smooths small-scale structures.

Table 3
TID Propagation Parameters Estimated Using the FFT and MEM Spectral Information Based on Reference Stations 1, 2, and 3

Method	Frequency (Hz)	Period (min)	Velocity (m/s)	Wavelength (km)	Azimuth (°)
FFT	0.000326	51.2	33.837	103.948	249.663
MEM	0.000326	51.2	34.159	104.938	249.305

15427390, 2026, 1, Downloaded from https://agupubs.onlinelibrary.wiley.com/doi/10.1029/2025SW004538 by Trinity Health Ann Arbor, Wiley Online Library on [01/04/2026]. See the Terms and Conditions (https://onlinelibrary.wiley.com/terms-and-conditions) on Wiley Online Library for rules of use; OA articles are governed by the applicable Creative Commons License

Table 4
TID Propagation Parameters Based on MEM Spectral Information for Different Station Combinations

Station combinations	Frequency (Hz)	Period (min)	Velocity (m/s)	Wavelength (km)	Azimuth (°)
1-2-4	0.000326	51.2	34.391	105.648	249.521
1-3-4	0.000326	51.2	32.325	99.301	251.389
2-3-4	0.000326	51.2	33.786	103.789	249.780

Note. Notably, these results align closely with the reference-station-derived parameters (see Table 3), demonstrating the model's capability to accurately estimate rover station TID signals using established propagation characteristics. This validation confirms the model's robustness for operational applications in regional TID monitoring networks.

3.3. Validation of TID Propagation Model

In this section, the TID propagation model was validated by using simulated and real GEO TEC data.

3.3.1. Validation by the Simulated TEC Data

The TID propagation model developed in Section 2.3 enables precise calculation of TID signals at arbitrary rover stations. As demonstrated in Figure 11, the model successfully simulates TID signals for three reference stations (TID1, TID2, and TID3). These results confirm that with accurate propagation parameters (amplitude, frequency, phase), the model can reliably reconstruct TID signals (TID4) at any rover location within the study area based on TID signals of reference stations. This capability significantly enhances our ability to characterize and mitigate TID effects across regional GNSS networks.

Figure 12 presents the original TEC and dTEC series at the HKTK station on 28 October 2018 (a geomagnetically quiet day). For model validation, we added the simulated TID signal (13:00–16:00 UT) derived from our propagation model into this original dTEC series, as shown in the shaded area in Figure 13. The simulated GEO dTEC time series exhibits pronounced fluctuations during the simulated period, successfully reproducing the expected TID signature while maintaining the background ionospheric characteristics. This simulated experiment demonstrates the model's ability to accurately represent TID-induced perturbations in dTEC series.

As shown in Table 3, based on the FFT spectral information, the estimated frequency using three reference stations 1, 2, and 3 is 0.000326 Hz, with a period of 51.2 min, a propagation speed of 33.837 m/s, a wavelength of 103.948 km, and a direction of 249.663°. Based on the MEM spectral information, the estimated frequency using three reference stations 1, 2, and 3 is 0.000326 Hz, with a period of 51.2 min, a propagation speed of 34.159 m/s, a wavelength of 104.938 km, and a direction of 249.305°.

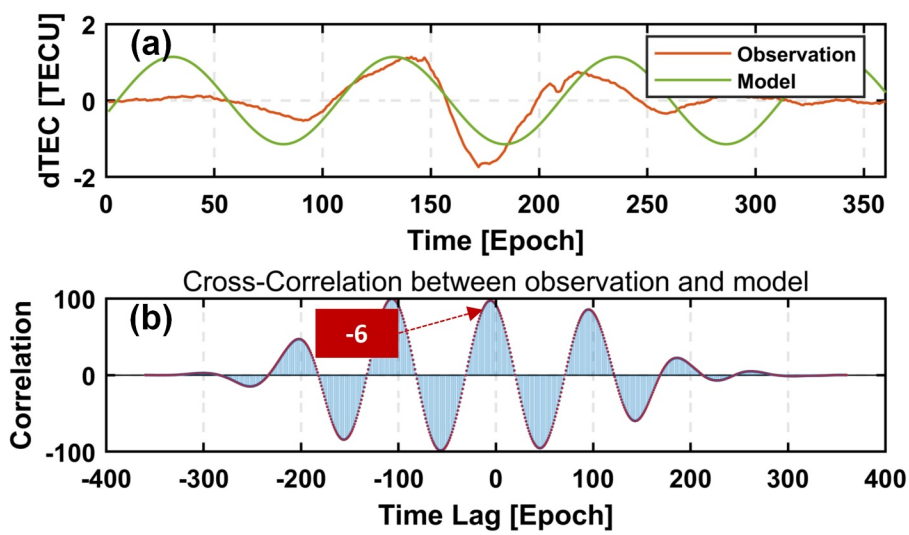

Figure 14. Comparison and cross-correlation analysis between the measured and model-estimated TID signals at the HKSC station on 29 October 2018.

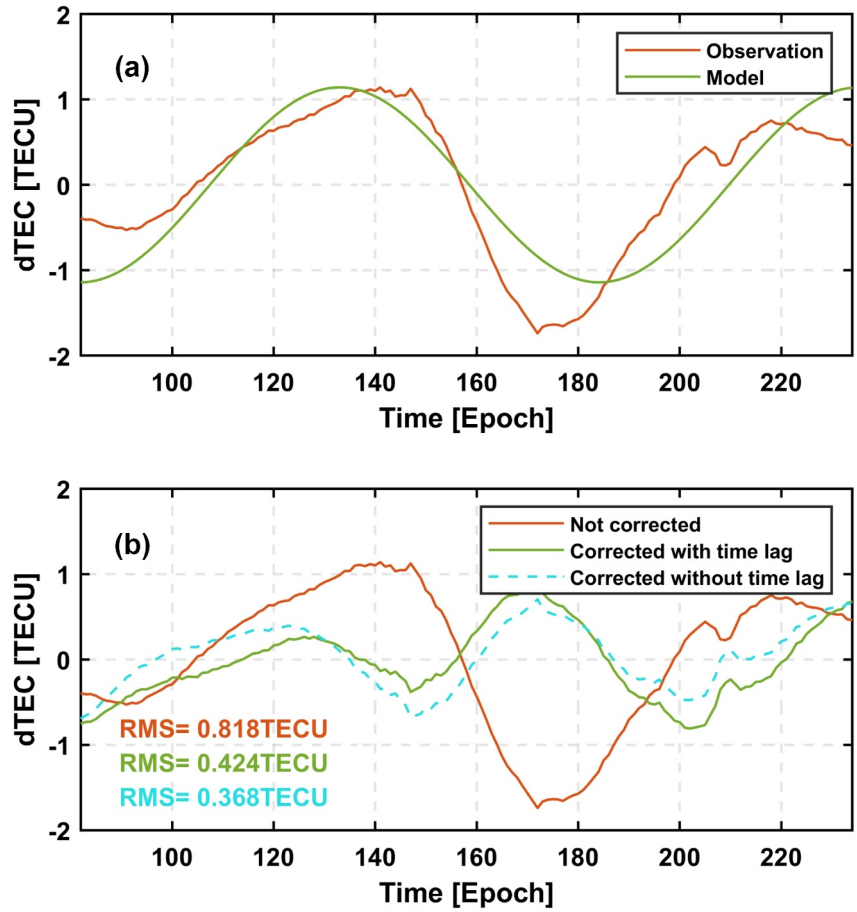

Figure 15. Comparison of the ionospheric delay errors before and after correcting the TID effects over HKSC station on 29 October 2018.

To assess the model's accuracy, we calculated TID parameters using rover station 4 paired with two different reference stations via MEM analysis. The results are presented in Table 4: (a) The estimated TID propagation frequency using the combination of reference stations 1 and 2 and rover station 4 is 0.000326 Hz, with a period of 51.2 min, a propagation speed of 34.391 m/s, a wavelength of 105.648 km, and a direction of 249.521°; (b) The estimated TID propagation frequency using the combination of reference stations 1, 3, and rover station 4 is 0.000326 Hz, with a period of 51.2 min, a propagation speed of 32.325 m/s, a wavelength of 99.301 km, and a direction of 251.389°; (c) The estimated TID propagation frequency using the combination of reference stations 2, 3, and rover station 4 is 0.000326 Hz, with a period of 51.2 min, a propagation speed of 33.786 m/s, a wavelength of 103.789 km, and a direction of 249.780°. Three different combinations consistently identified the same frequency characteristics (0.000326 Hz), with propagation parameters showing remarkable consistency.

3.3.2. Validation by Real GEO TEC Data

In order to verify the accuracy and reliability of the propagation model, the measured TID signal of a complete cycle (including one peak and one trough) at the HKSC station on 29 October 2018 was extracted, and the TID signal at the HKSC station during the same period was estimated using the propagation model. Figure 14 presents the comparative and cross-correlation analysis between the observed and model-estimated dTEC variations at the HKSC station during the TID event period (13:00–16:00 UT, epochs 1560–1920). It shows strong agreement between the model-estimated and measured TID signals. As shown in Figure 14b, we noted that there is a time lag between the observed and model-estimated TID signals, and the six-epoch (3-min) time lag was identified through cross-correlation analysis.

15427390, 2026, 1, Downloaded from https://agupubs.onlinelibrary.wiley.com/doi/10.1029/2025SW004538 by Trinity Health Ann Arbor, Wiley Online Library on [01/04/2026]. See the Terms and Conditions (https://onlinelibrary.wiley.com/terms-and-conditions) on Wiley Online Library for rules of use; OA articles are governed by the applicable Creative Commons License

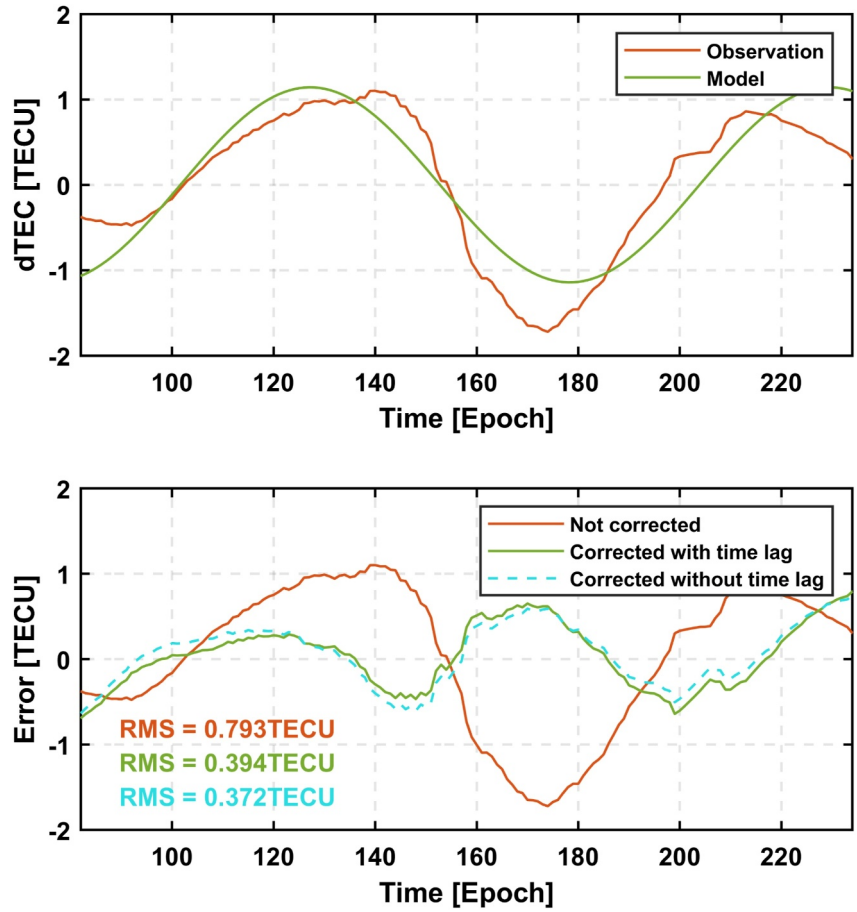

Figure 16. Comparison of the ionospheric delay errors before and after correcting the TID effects over HKST station on 29 October 2018.

Figure 15 validates the TID propagation model through a complete cycle comparison with the measured TID signal at the HKSC station. The model successfully reproduces both the waveform morphology and amplitude variations of the measured TID signal (see the top panel of Figure 15). The modeled signal effectively captures the complete wave structure (peak-trough sequence), enabling precise TID effect compensation and correction. Figure 15 also compares the ionospheric delay error variations before and after correcting the TID effect at the HKSC station. The correction results demonstrate significant mitigation of TID-induced ionospheric delay errors, reducing the RMS value of ionospheric delay from 0.818 TECU (uncorrected) to 0.424 TECU (48.2% improvement) without accounting for the observed six-epoch time lag, and further to 0.368 TECU (55.0% improvement) with optimal temporal alignment (see the bottom panel of Figure 15). The 6.8% performance difference between these correction approaches underscores the importance of precise phase matching in TID mitigation strategies, while the overall results confirm the model's operational effectiveness for regional ionospheric disturbance correction.

Figures 16 and 17 also compare the ionospheric delay error variations through a complete cycle before and after correcting the TID effect at the HKST and HKKT stations, respectively. In Figure 16, the correction results over HKST station demonstrate mitigation of TID-induced ionospheric delay errors, reducing the RMS value of ionospheric delay from 0.793 TECU (uncorrected) to 0.394 TECU (50.3% improvement) without accounting for the observed three-epoch time lag, and further to 0.372 TECU (53.1% improvement) with optimal temporal alignment. In Figure 17, the correction results over HKKT station also demonstrate mitigation of TID-induced ionospheric delay errors, reducing the RMS value of ionospheric delay from 0.736 TECU (uncorrected) to 0.422 TECU (42.7% improvement) without accounting for the observed two-epoch time lag, and further to 0.404

15427390, 2026, 1, Downloaded from https://agupubs.onlinelibrary.wiley.com/doi/10.1029/2025SW004538 by Trinity Health Ann Arbor, Wiley Online Library on [01/04/2026]. See the Terms and Conditions (https://onlinelibrary.wiley.com/terms-and-conditions) on Wiley Online Library for rules of use; OA articles are governed by the applicable Creative Commons License

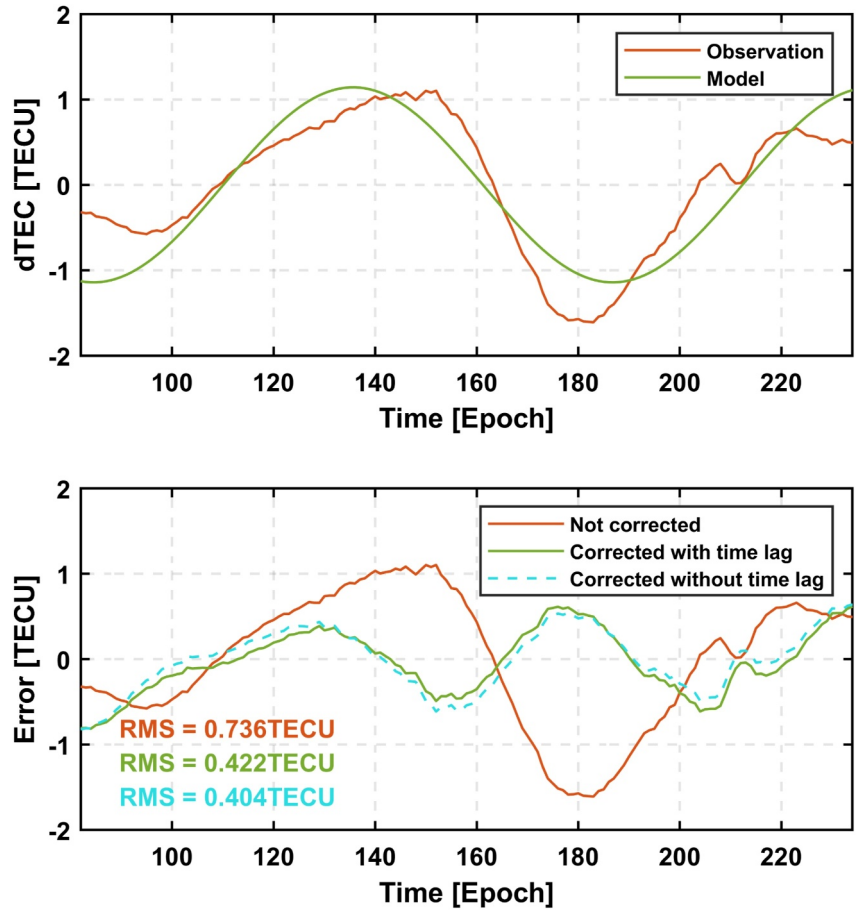

Figure 17. Comparison of the ionospheric delay errors before and after correcting the TID effects over HKKT station on 29 October 2018.

TECU (45.1% improvement) with optimal temporal alignment. The results confirm the model's operational effectiveness for regional traveling ionospheric disturbance correction.

Besides, we selected a typical nighttime MSTID event that occurred between 04:00 UT (Epoch 480) and 07:00 UT (Epoch 840) on 30 April 2016. This event was reported in our previous study (Le et al., 2024) and exhibited propagation parameters that differ from those of the aforementioned MSTID event on 29 October 2018. Based on the dTEC sequences derived from the HKCL-HKLM-HKSS station combination (Figure 18), the propagation parameters of the MSTID were estimated using the same cross-spectral method. The derived TID propagation parameters—a period of 23.27 min, a velocity of 160.65 m/s, a wavelength of 224.32 km, and a propagation direction of 189.17°—were then used to construct a TID propagation model for station HKPC.

Figure 19 compares the model-estimated TID series with the observed TID series over three consecutive wave cycles. The results show that the modeled TID variations closely match the observed ones. When the model-estimated TID values were used to correct the observed TID signal, the RMS of the TID-induced ionospheric delay error was reduced from 0.258 TECU to 0.153 TECU, a reduction of approximately 40.7%. In this case, since no significant time lag existed between the modeled and observed TID signals, only the scenario without time delay correction was discussed.

The two different MSTID events collectively demonstrates that the proposed TID model can reliably reconstruct TID signals at rover stations, even under different propagation characteristics. It should be noted that the integrated GNSS-derived TEC naturally smooths smaller-scale structures and can only capture the integrated TEC perturbations along satellite-receiver ray path. Therefore, our regional cosine-based model represents an effective

15427390, 2026, 1, Downloaded from https://agupubs.onlinelibrary.wiley.com/doi/10.1029/2025SW004538 by Trinity Health Ann Arbor, Wiley Online Library on [01/04/2026]. See the Terms and Conditions (https://onlinelibrary.wiley.com/terms-and-conditions) on Wiley Online Library for rules of use; OA articles are governed by the applicable Creative Commons License

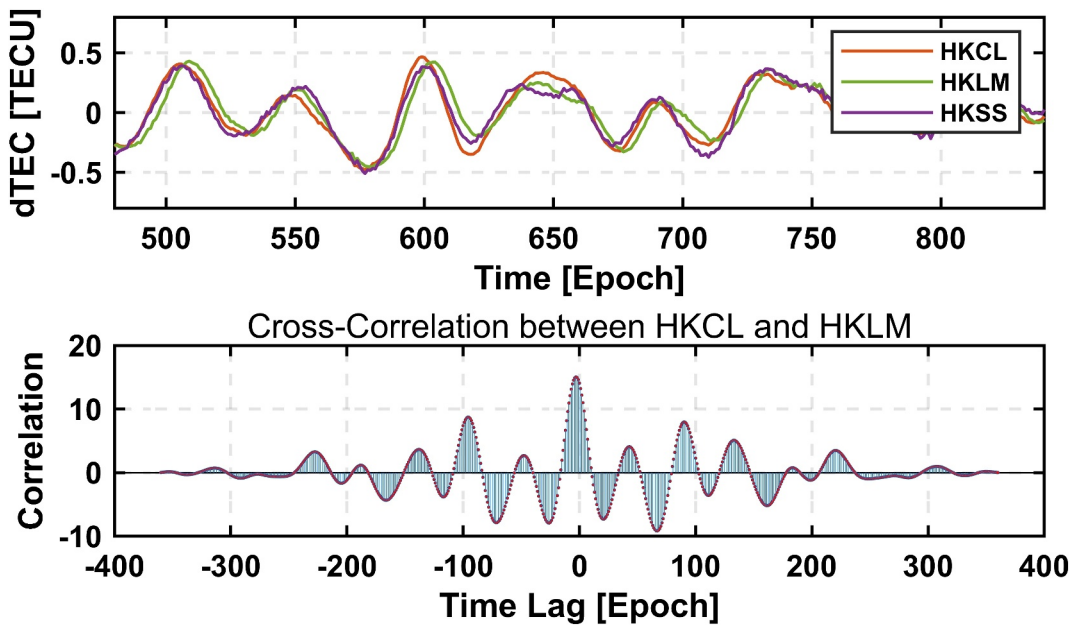

Figure 18. Comparison and cross-correlation analysis between the measured TID signals at the HKCL, HKLM, and HKSS stations on 30 April 2016.

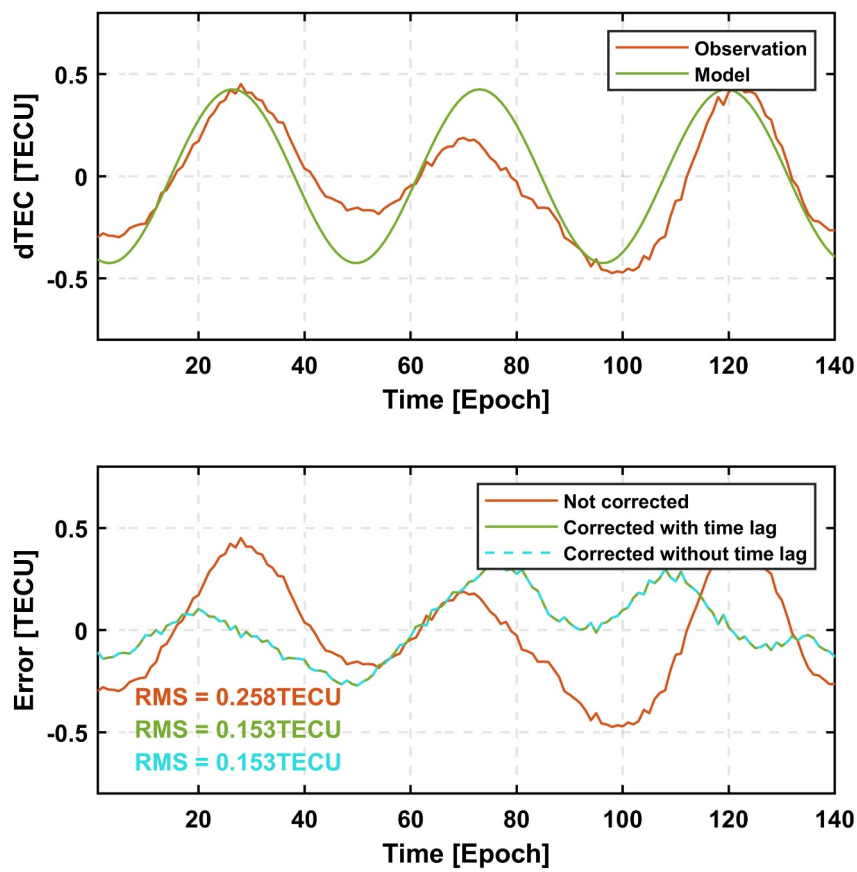

Figure 19. Comparison of the ionospheric delay errors before and after correcting the TID effects over HKPC station on 30 April 2016.

15427390, 2026, 1, Downloaded from https://agupubs.onlinelibrary.wiley.com/doi/10.1029/2025SW004538 by Trinity Health Ann Arbor, Wiley Online Library on [01/04/2026]. See the Terms and Conditions (https://onlinelibrary.wiley.com/terms-and-conditions) on Wiley Online Library for rules of use; OA articles are governed by the applicable Creative Commons License

15427390, 2026, 1, Downloaded from https://agupubs.onlinelibrary.wiley.com/doi/10.1029/2025SW004538 by Trinity Health Ann Arbor, Wiley Online Library on [01/04/2026]. See the Terms and Conditions (https://onlinelibrary.wiley.com/terms-and-conditions) on Wiley Online Library for rules of use; OA articles are governed by the applicable Creative Commons License

approximation that captures the dominant wave mode. Besides, the results from three testing cases confirm that the simplified single-wave model accurately characterized primary wavefront propagation.

4. Conclusion and Future Work

Traveling ionospheric disturbances cause electron density perturbations that can significantly degrade the accuracy and reliability of GNSS precise positioning. This study has developed and validated a regional TID propagation model using BDS GEO TEC observations, demonstrating significant improvements in ionospheric delay correction accuracy through mitigation of TID effects. The key conclusions are as follows:

1. The proposed SSA-based data gap filling method successfully addresses possible data discontinuity issues in BDS GEO TEC observations, enabling reliable continuous monitoring of TID events. The refined cross-spectral analysis approach provides robust estimation of TID propagation parameters by grouping geometrically well-distributed reference stations into triplets and averaging the derived parameters.
2. The cosine-function-based propagation model effectively characterizes TID disturbances through integration of phase, frequency, and amplitude information. The propagation model performances were evaluated by both simulated and real BDS GEO TEC data. Validation results on 29 October 2018 show the model reduces TID-induced ionospheric delay errors by 48.2%, 50.3%, and 42.7% without accounting for the time lag and further by 55.0%, 53.1%, and 45.1% with optimal temporal alignment for HKSC, HKST, and HKKT, respectively. The performance difference between time-lag and time-aligned corrections quantitatively demonstrates the importance of precise phase matching in TID mitigation. Another validation experiment was conducted by selecting a typical MSTID event that occurred on 30 April 2016. This MSTID event exhibited different propagation parameters. The results show that the model can reduce the TID-induced ionospheric delay errors by 40.7%. These results validate the model's operational effectiveness while highlighting potential enhancements through improved temporal alignment techniques. It also demonstrates that the proposed TID model can reliably reconstruct TID signals at rover stations, even under different propagation characteristics.

The proposed methodology advances GNSS positioning accuracy in TID-affected regions and contributes to ionospheric research through its data-driven modeling approach. Future work should focus on extending validation under geomagnetic conditions and developing adaptive temporal alignment algorithms, as well as investigating GNSS precise positioning performances by correcting TID effects with TID propagation model. These developments would further enhance the model's utility for both operational GNSS applications and scientific studies of ionospheric dynamics.

Conflict of Interest

The authors declare no conflicts of interest relevant to this study.

Data Availability Statement

The GNSS RINEX data is obtained from Hong Kong Geodetic Survey Services (https://www.geodetic.gov.hk/en/rinex/downv.aspx). The open-source code of the singular spectrum analysis (SSA) gap-filling technique is available via (Yi & Sneeuw, 2021b).

Acknowledgments
This study was supported by the National Natural Science Foundation of China (42504024, 42230104) and the National Science Fund for Distinguished Young Scholars of China (42425003). It was also supported by the National Funded Postdoctoral Researchers Program (GZC20250170) and LIESMARS Special Research Funding, the Open Fund of the Key Laboratory of Polar Environment Monitoring and Public Governance (PEMPG), Ministry of Education, China (202510). The numerical calculations have been done on the supercomputing system in the Supercomputing Center of Wuhan University.

References

Banville, S., & Langley, R. B. (2013). Mitigating the impact of ionospheric cycle slips in GNSS observations. *Journal of Geodesy*, *87*(2), 179–193. https://doi.org/10.1007/s00190-012-0604-1

Basu, S., Groves, K., Basu, S., & Sultan, P. (2002). Specification and forecasting of scintillations in communication/navigation links: Current status and future plans. *Journal of Atmospheric and Solar-Terrestrial Physics*, *64*(16), 1745–1754. https://doi.org/10.1016/s1364-6826(02)00124-4

Belehaki, A., Tsagouri, I., Altadill, D., Blanch, E., Borries, C., Buresova, D., et al. (2020). An overview of methodologies for real-time detection, characterisation and tracking of traveling ionospheric disturbances developed in the TechTIDE project. *Journal of Space Weather and Space Climate*, *10*, 42. https://doi.org/10.1051/swsc/2020043

Chen, G., Ding, F., Wan, W., Hu, L., Zhao, X., & Li, J. (2020). Structures of multiple large-scale traveling ionospheric disturbances observed by dense Global Navigation Satellite System networks in China. *Journal of Geophysical Research: Space Physics*, *125*(2), e2019JA027032. https://doi.org/10.1029/2019ja027032

Chen, P., Xiong, M., Wang, R., Yao, Y., Tang, F., Chen, H., & Qiu, L. (2023). On the ionospheric disturbances in New Zealand and Australia following the eruption of the Hunga Tonga-Hunga Ha'apai volcano on 15 January 2022. *Space Weather*, *21*(4), e2022SW003294. https://doi.org/10.1029/2022sw003294

Ding, F., Wan, W., Ning, B., & Wang, M. (2007). Large-scale traveling ionospheric disturbances observed by GPS total electron content during the magnetic storm of 29-30 October 2003. *Journal of Geophysical Research*, *112*(A6). https://doi.org/10.1029/2006ja012013

Ding, F., Wan, W., Xu, G., Yu, T., Yang, G., & Wang, J. S. (2011). Climatology of medium-scale traveling ionospheric disturbances observed by a GPS network in central China. *Journal of Geophysical Research*, *116*(A9). https://doi.org/10.1029/2011ja016545

Frissell, N. A., Baker, J. B. H., Ruohoniemi, J. M., Greenwald, R. A., Gerrard, A. J., Miller, E. S., & West, M. L. (2016). Sources and characteristics of medium-scale traveling ionospheric disturbances observed by high-frequency radars in the North American sector. *Journal of Geophysical Research: Space Physics*, *121*(4), 3722–3739. https://doi.org/10.1002/2015ja022168

Gou, J., Kiani Shahvandi, M., Hohensinn, R., & Soja, B. (2023). Ultra-short-term prediction of LOD using LSTM neural networks. *Journal of Geodesy*, *97*(5), 52. https://doi.org/10.1007/s00190-023-01745-x

Hajkowicz, L. A. (1990). A global study of large scale travelling ionospheric disturbances (TIDs) following a step-like onset of auroral substorms in both hemispheres. *Planetary and Space Science*, *38*(7), 913–923. https://doi.org/10.1016/0032-0633(90)90058-x

Hernández-Pajares, M., Juan, J. M., & Sanz, J. (2006). Medium-scale traveling ionospheric disturbances affecting GPS measurements: Spatial and temporal analysis. *Journal of Geophysical Research*, *111*(A7). https://doi.org/10.1029/2005ja011474

Hernández-Pajares, M., Wielgosz, P., Paziewski, J., Krypiak-Gregorczyk, A., Krukowska, M., Stepniak, K., et al. (2017). Direct MSTID mitigation in precise GPS processing. *Radio Science*, *52*(3), 321–337. https://doi.org/10.1002/2016rs006159

Huang, F., Dou, X., Lei, J., Lin, J., Ding, F., & Zhong, J. (2016). Statistical analysis of nighttime medium-scale traveling ionospheric disturbances using airglow images and GPS observations over central China. *Journal of Geophysical Research: Space Physics*, *121*(9), 8887–8899. https://doi.org/10.1002/2016ja022760

Huang, F., Lei, J., Dou, X., Luan, X., & Zhong, J. (2018). Nighttime medium-scale traveling ionospheric disturbances from airglow imager and Global Navigation Satellite Systems observations. *Geophysical Research Letters*, *45*(1), 31–38. https://doi.org/10.1002/2017gl076408

Huang, F., Lei, J., Otsuka, Y., Luan, X., Liu, Y., Zhong, J., & Dou, X. (2020). Characteristics of medium-scale traveling ionospheric disturbances and ionospheric irregularities at mid-latitudes revealed by the total electron content associated with the Beidou geostationary satellite. *IEEE Transactions on Geoscience and Remote Sensing*, *59*(8), 6424–6430. https://doi.org/10.1109/tgrs.2020.3032741

Jia, H., Yang, Z., & Li, B. (2024). ROTI-based statistical regression models for GNSS precise point positioning errors associated with ionospheric plasma irregularities. *GPS Solutions*, *28*(3), 105. https://doi.org/10.1007/s10291-024-01648-0

Kelley, M. (2011). On the origin of mesoscale TIDs at midlatitudes. *Annales Geophysicae*, *29*(2), 361–366. https://doi.org/10.5194/angeo-29-361-2011

Kondrashov, D., & Ghil, M. (2006). Spatio-temporal filling of missing points in geophysical data sets. *Nonlinear Processes in Geophysics*, *13*(2), 151–159. https://doi.org/10.5194/npg-13-151-2006

Kotake, N., Otsuka, Y., Ogawa, T., Tsugawa, T., & Saito, A. (2007). Statistical study of medium-scale traveling ionospheric disturbances observed with the GPS networks in Southern California. *Earth Planets and Space*, *59*(2), 95–102. https://doi.org/10.1186/bf03352681

Kotake, N., Otsuka, Y., Tsugawa, T., Ogawa, T., & Saito, A. (2006). Climatological study of GPS total electron content variations caused by medium-scale traveling ionospheric disturbances. *Journal of Geophysical Research*, *111*(A4). https://doi.org/10.1029/2005ja011418

Le, X., Ren, X., Mei, D., Liu, H., & Zhang, X. (2024). Occurrence and characteristics of medium-scale traveling ionospheric disturbances observed by BeiDou GEO satellites over Hong Kong. *Journal of Geophysical Research: Space Physics*, *129*(6), e2024JA032510. https://doi.org/10.1029/2024ja032510

Lee, J., Morton, Y. J., Lee, J., Moon, H.-S., & Seo, J. (2017). Monitoring and mitigation of ionospheric anomalies for GNSS-based safety critical systems: A review of up-to-date signal processing techniques. *IEEE Signal Processing Magazine*, *34*(5), 96–110. https://doi.org/10.1109/msp.2017.2716406

Li, F., Kusche, J., Rietbroek, R., Wang, Z., Forootan, E., Schulze, K., & Lück, C. (2020). Comparison of data-driven techniques to reconstruct (1992–2002) and predict (2017–2018) GRACE-like gridded total water storage changes using climate inputs. *Water Resources Research*, *56*(5), e2019WR026551. https://doi.org/10.1029/2019wr026551

Li, G., Ning, B., Otsuka, Y., Abdu, M. A., Abadi, P., Liu, Z., et al. (2021). Challenges to equatorial plasma bubble and ionospheric scintillation short-term forecasting and future aspects in east and southeast Asia. *Surveys in Geophysics*, *42*(1), 201–238. https://doi.org/10.1007/s10712-020-09613-5

Li, W., Wang, W., Zhang, C., Wen, H., Zhong, Y., Zhu, Y., & Li, Z. (2019). Bridging terrestrial water storage anomaly during GRACE/GRACE-FO gap using SSA method: A case study in China. *Sensors*, *19*(19), 4144. https://doi.org/10.3390/s19194144

Li, X., Huang, J., Li, X., Shen, Z., Han, J., Li, L., & Wang, B. (2022). Review of PPP–RTK: Achievements, challenges, and opportunities. *Satellite Navigation*, *3*(1), 28. https://doi.org/10.1186/s43020-022-00089-9

Liu, Y., Zhou, C., Tang, Q., Kong, J., Gu, X., Ni, B., et al. (2019). Evidence of mid-and low-latitude nighttime ionospheric E-F coupling: Coordinated observations of sporadic E layers, F-region field-aligned irregularities, and medium-scale traveling ionospheric disturbances. *IEEE Transactions on Geoscience and Remote Sensing*, *57*(10), 7547–7557. https://doi.org/10.1109/tgrs.2019.2914059

Mei, D., Zhang, X., Ren, X., Le, X., Liu, H., & Freeshah, M. (2025). Two-and three-dimensional propagation characteristics of co-volcanic ionospheric disturbances induced by the 2022 Tonga volcano eruption using dense GNSS network data. *Journal of Geophysical Research: Space Physics*, *130*(1), e2024JA032488. https://doi.org/10.1029/2024ja032488

Paziewski, J., Høeg, P., Sieradzki, R., Jin, Y., Jarmolowski, W., Hoque, M. M., et al. (2022). The implications of ionospheric disturbances for precise GNSS positioning in Greenland. *Journal of Space Weather and Space Climate*, *12*, 33. https://doi.org/10.1051/swsc/2022029

Perkins, F. (1973). Spread F and ionospheric currents. *Journal of Geophysical Research*, *78*(1), 218–226. https://doi.org/10.1029/ja078i001p00218

Ren, X., Mei, D., Liu, H., & Zhang, X. (2022). Investigation on horizontal and vertical traveling ionospheric disturbances propagation in global-scale using GNSS and multi-LEO satellites. *Space Weather*, *20*(5), e2022SW003041. https://doi.org/10.1029/2022sw003041

Schoellhamer, D. H. (2001). Singular spectrum analysis for time series with missing data. *Geophysical Research Letters*, *28*(16), 3187–3190. https://doi.org/10.1029/2000gl012698

Shiokawa, K., Ihara, C., Otsuka, Y., & Ogawa, T. (2003). Statistical study of nighttime medium-scale traveling ionospheric disturbances using midlatitude airglow images. *Journal of Geophysical Research*, *108*(A1). https://doi.org/10.1029/2002ja009491

Sun, A. Y., Scanlon, B. R., Zhang, Z., Walling, D., Bhanja, S. N., Mukherjee, A., & Zhong, Z. (2019). Combining physically based modeling and deep learning for fusing GRACE satellite data: Can we learn from mismatch? *Water Resources Research*, *55*(2), 1179–1195. https://doi.org/10.1029/2018wr023333

Tang, L. (2023). Ionospheric disturbances of the January 15, 2022, Tonga volcanic eruption observed using the GNSS network in New Zealand. *GPS Solutions*, *27*(1), 53. https://doi.org/10.1007/s10291-023-01395-8

15427390, 2026, 1, Downloaded from https://agupubs.onlinelibrary.wiley.com/doi/10.1029/2025SW004538 by Trinity Health Ann Arbor, Wiley Online Library on [01/04/2026]. See the Terms and Conditions (https://onlinelibrary.wiley.com/terms-and-conditions) on Wiley Online Library for rules of use; OA articles are governed by the applicable Creative Commons License

Timoté, C. C., Juan, J. M., Sanz, J., González-Casado, G., Rovira-García, A., & Escudero, M. (2020). Impact of medium-scale traveling ionospheric disturbances on network real-time kinematic services: CATNET study case. *Journal of Space Weather and Space Climate*, *10*, 29. https://doi.org/10.1051/swsc/2020030

Tsuboi, T., Shiokawa, K., Otsuka, Y., Fujinami, H., Nakamura, T., & Neudegg, D. (2023). Statistical analysis of the horizontal phase velocity distribution of atmospheric gravity waves and medium-scale traveling ionospheric disturbances in airglow images over Darwin (12.4°S, 131.0°E). *Journal of Geophysical Research: Space Physics*, *128*(8), e2022JA030769. https://doi.org/10.1029/2022ja030769

Tsugawa, T., Kotake, N., Otsuka, Y., & Saito, A. (2007). Medium-scale traveling ionospheric disturbances observed by GPS receiver network in Japan: A short review. *GPS Solutions*, *11*(2), 139–144. https://doi.org/10.1007/s10291-006-0045-5

Vilà-Valls, J., Linty, N., Closas, P., Dovis, F., & Curran, J. T. (2020). Survey on signal processing for GNSS under ionospheric scintillation: Detection, monitoring, and mitigation. *Navigation: Journal of the Institute of Navigation*, *67*(3), 511–535.

Wan, W., Ning, B., Yuan, H., Li, J., Li, L., & Liang, J. (1997). TID observation using a short baseline network of GPS receivers. *Acta Geodaetica et Geophysica Hungarica*, *32*(3–4), 321–327. https://doi.org/10.1007/bf03325503

Wu, K., Xu, J., Wang, W., Sun, L., & Yuan, W. (2021). Interaction of oppositely traveling medium-scale traveling ionospheric disturbances observed in low latitudes during geomagnetically quiet nighttime. *Journal of Geophysical Research: Space Physics*, *126*(2), e2020JA028723. https://doi.org/10.1029/2020ja028723

Yang, H., Monte-Moreno, E., & Hernández-Pajares, M. (2017). Multi-TID detection and characterization in a dense Global Navigation Satellite System receiver network. *Journal of Geophysical Research: Space Physics*, *122*(9), 9554–9575. https://doi.org/10.1002/2017ja023988

Yang, Z., & Morton, Y. J. (2020). Low-latitude GNSS ionospheric scintillation dependence on magnetic field orientation and impacts on positioning. *Journal of Geodesy*, *94*(6), 59. https://doi.org/10.1007/s00190-020-01391-7

Yi, S., & Sneeuw, N. (2021a). Filling the data gaps within GRACE missions using singular spectrum analysis. *Journal of Geophysical Research: Solid Earth*, *126*(5), e2020JB021227. https://doi.org/10.1029/2020jb021227

Yi, S., & Sneeuw, N. (2021b). Data for: Filling the data gaps within GRACE missions using Singular Spectrum Analysis [Dataset]. *DaRUS, V1*. https://doi.org/10.18419/DARUS-807

Zakharenkova, I., Astafyeva, E., & Cherniak, I. (2016). GPS and GLONASS observations of large-scale traveling ionospheric disturbances during the 2015 St. Patrick's Day storm. *Journal of Geophysical Research: Space Physics*, *121*(12), 12138–112156. https://doi.org/10.1002/2016ja023332

Zhai, C., Zhang, S. R., Yao, Y., Dong, W., Aa, E., Kong, J., et al. (2025). Three-dimensional characterization of global ionospheric disturbances during the 15 January 2022 Tonga volcanic eruption. *Geophysical Research Letters*, *52*(2), e2024GL113129. https://doi.org/10.1029/2024gl113129

Zhang, X., Ren, X., Chen, J., Zuo, X., Mei, D., & Liu, W. (2022). Investigating GNSS PPP–RTK with external ionospheric constraints. *Satellite Navigation*, *3*(1), 6. https://doi.org/10.1186/s43020-022-00067-1

15427390, 2026, 1, Downloaded from https://agupubs.onlinelibrary.wiley.com/doi/10.1029/2025SW004538 by Trinity Health Ann Arbor, Wiley Online Library on [01/04/2026]. See the Terms and Conditions (https://onlinelibrary.wiley.com/terms-and-conditions) on Wiley Online Library for rules of use; OA articles are governed by the applicable Creative Commons License